PERFORMANCE OF A 1.3 GHZ NORMAL-CONDUCTING 5-CELL STANDING-WAVE CAVITY*

Faya Wang, Chris Adolphsen and Juwen Wang, SLAC, Menlo Park, CA 94025, U.S.A

Abstract

A 5-cell, normal-conducting, 1.3 GHz, standing-wave (SW) cavity was built as a prototype capture accelerator for the ILC positron source. Although the ILC uses predominately superconducting cavities, the capture cavity location in both a high radiation environment and a solenoidal magnetic field requires it to be normal conducting. With the relatively high duty ILC beam pulses (1 msec at 5 Hz) and the high gradient required for efficient positron capture (15 MV/m), achieving adequate cavity cooling to prevent significant detuning is challenging. This paper presents the operational performance of this cavity including the processing history, characteristics of the breakdown events and the acceleration gradient witnessed by a single bunch at different injection times for different rf pulse lengths.

INTRODUCTION

Due to high radiation levels and the need of a solenoidal magnetic field for focusing, the 1.3 GHz pre-accelerator that follows the ILC positron target will be normal conducting. A half-length (5-cell) prototype standing-wave (SW), cavity was built at SLAC to verify that the gradient (15 MV/m in 1.0 ms pulses) can be achieved stably and without significant detuning from the RF heat load (4 kW per cell). Details of the design can be found in [1, 2], and the cavity cross-section is shown in Fig. 1 [3].

Fig. 2 is a plot of the cold test measurement of the mode frequencies (dots); the solid line is the fitted dispersion curve, expressed as,

$$f_n^2 = \frac{f_0^2}{1 + k_1 \cos(\phi)}$$

with f_0= 1291.8 MHz and k_1= 0.01249. The unloaded Q of the cavity is ~ 29000 and the operating frequency (at π phase advance) is 1299.7 MHz. The time constant of this critically-coupled cavity ($0.5Q_o/\omega$) is 1.8 us.

So far, the cavity has been rf processed at the π-mode for about 530 hrs and it has incurred about 6200 breakdowns. The gradient goal of 15 MV/m with 1 ms pulses has been achieved. Fig. 3 shows the breakdown rate history during processing. For these data, the pulse repetition rate was 5 Hz except for 1 ms pulses where it was lowered to 1 Hz to reduce the detuning as the reflected power was causing waveguide breakdowns (the source of these breakdowns has since been eliminated and 5 Hz operation is expected to be possible in the future).

The goal when designing the cavity cooling system was to have about 25% reflected power when the cavity was turned on 'cold' that then dropped to zero in steady state with full rf power dissipation (20 kW at 15 MV/m). In this way, a cavity temperature control system is not needed (at least for testing). However, the flow rate that was achieved (due to a limited supply of temperature-regulated water) was 86 gpm compared to the 140 gpm desired, which increased the cavity temperature by about 50% (to 0.13 degC per kW dissipated). Also, the detuning (-2.7 kHz/kW) was about 25% larger than expected from simulations using the actual temperature rise and led to an overall reflection of about 50% when cold with the appropriate choice of rf frequency to minimize the reflection at full power in steady state.

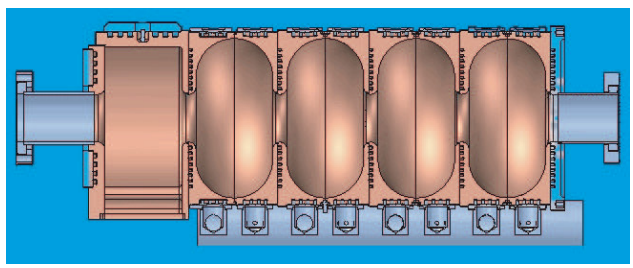

Figure. 1: Cross sectional view of the 5-cell cavity where the coupler cell is on the left. Water circulates through rectangular grooves in the irises and outer cavity walls.

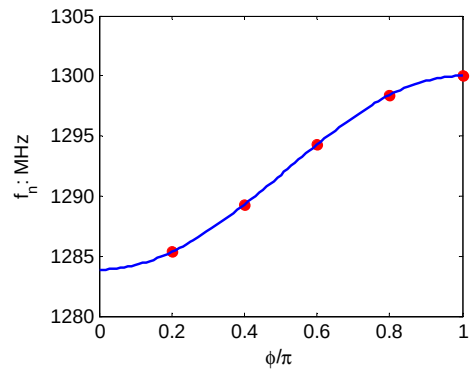

Figure 2: The 5-cell SW cavity dispersion curve.

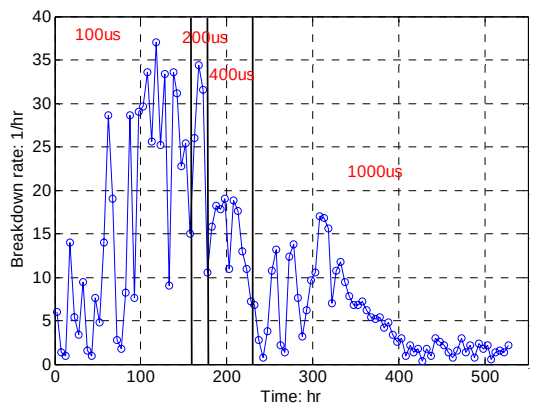

Figure 3: Breakdown rate history of the cavity for various pulse lengths (in red).

* Work Supported by DOE Contract DE-AC03-76F00515.

CAVITY BREAKDOWN STUDIES

After hundreds of hours of conditioning, the breakdown rate was measured as a function of unloaded gradient (G). A G^{21} dependence was found, which is less steep than the G^{32} dependence recently observed for a CERN-designed, low a/λ, TW, X-band (11.4 GHz) structure [4]. However, the gradient exponent is within the 20-30 range measured for NLC/GLC X-band prototype structures and close to the 19.5 value measured for the FNAL 805 MHz injector linac cavities.

The breakdowns fall into two types, which we call 'hard' and 'soft' depending on the decay profile of the cavity stored energy as measured by a pick-up probe in the beam pipe on the non-coupler end of the cavity. For hard events the stored energy drops quickly (in < 2 us) after a breakdown as illustrated in Fig. 4; for soft events it decays slowly (in 10-20 us), with a 'beating' pattern as illustrated in Fig. 5 (note: the actual beating frequency is higher than seen in the plot due to the low waveform sampling frequency, and the klystron power is shut off within 2 us after a breakdown is detected).

Although the cause for these two types of events is not known, one guess is that a breakdown effectively splits the cavity into two isolated parts, and the breakdown induced currents load the two parts differently in the two cases. That is, if the currents load down the non-coupler end, both the reflected power and stored energy fall rapidly (the reflected power because of the lower loaded *Q* and the stored energy because of the loading). If the currents load down the coupler end, however, the reflected power falls quickly, but the stored energy in the non-coupler end behaves as if it is in a shorter, higher *Q* cavity. In this case the stored energy drops slower, and because the energy is partitioned into more than one mode, there is a beating pattern as the energy decays.

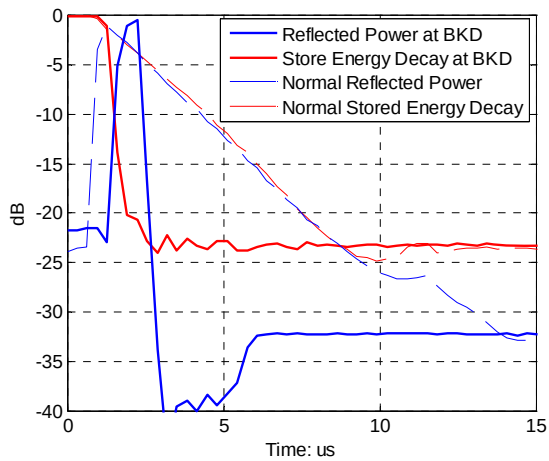

Figure 4: An example of a hard event. The red and blue dashed lines are the stored energy and reflected power, respectively, when the cavity turns off at the end of the pulse (no breakdown), and the solid lines are these waveforms for a breakdown event where the time scale has been shifted to match the initial drop in stored energy for the normal turn-off case.

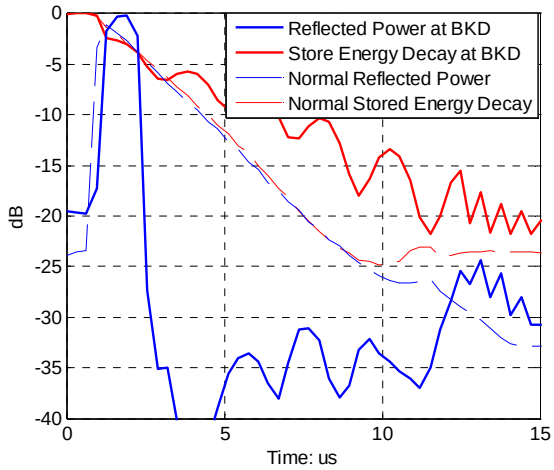

Figure 5: An example of a soft event. The waveforms are the same as described in the Fig. 4 caption.

To explore this further, an equivalent circuit model was used to analyze the transient response of the two cavity parts. The model shows that the stored energy remaining in each part will excite all possible modes in that part to some degree. For the coupler-end part, the loaded *Q* is quite low because of the coupler, so it is hard to see the oscillation in the reflected power after a breakdown. For the soft events, Fig. 6 shows the FFT of the simulated stored energy waveform when different irises are blocked (zero coupling through the iris) in the equivalent circuit model. By comparing the measured beating frequency with the peak values predicted, the breakdown iris should be identifiable. Since the waveforms shown were sampled at 3.125 MHz and there was some cross talk between the phase and amplitude, it is hard to extract the correct mode beating frequency from these data. In the future, a much higher sampling frequency will be used to study the breakdown waveforms. Finally, it is interesting to note how the fraction of hard and soft events changed during processing (see Fig.7).

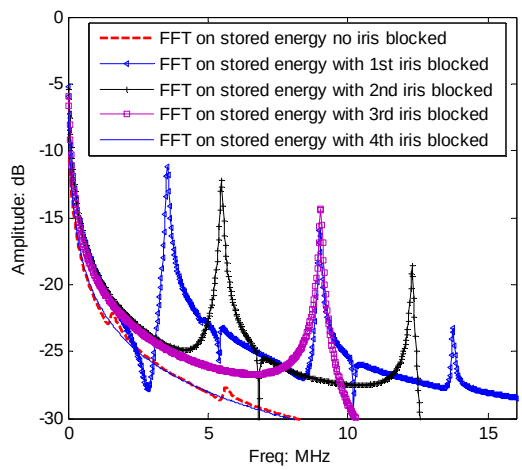

Figure 6: Predicted stored energy frequency spectrum at the non-coupler end of cavity when different irises are blocked.

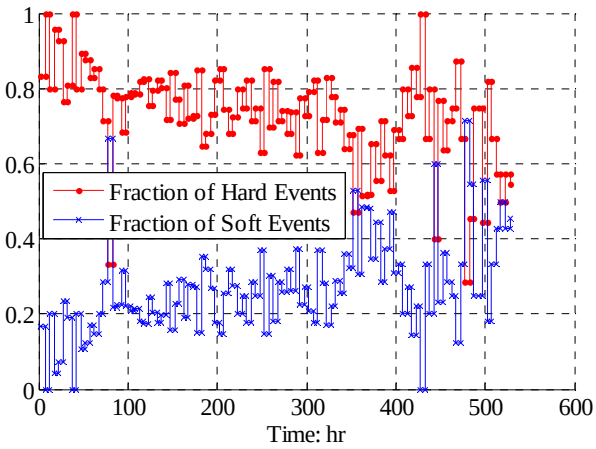

Figure 7: Hard and soft event fractions during conditioning.

DETUNING EFFECTS

To study how the detuning from average heating (up to 45 kHz at 15 MV/m) and intra-pulse heating (up to 4 kHz at 15 MV/m) affects the cavity gradient, the cell field distributions as a function of the detuning were computed using an equivalent circuit model. These data are shown in Fig. 8 together with the relative average gradient that a speed-of-light particle would see if the rf phase is optimized. This latter curve shows that the gradient is fairly independent of the frequency shifts in the range that are expected.

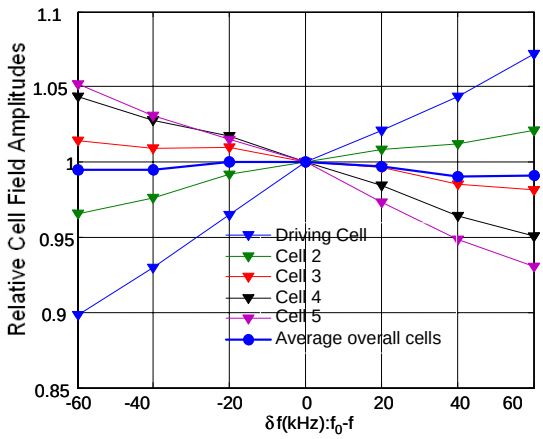

Figure 8: Simulated relative cell field amplitudes versus cavity detuning for a fixed net power into the cavity.

To explore the detuning effect experimentally, a single bunch was accelerated at 5 Hz in the cavity at NLCTA at different injection times (85 us and 900 us) during rf pulses with different widths (100 us and 1100 us). These combinations were chosen to distinguish detuning effects from low average heating, high average heating and intra-pulse heating. The gradients inferred from the bunch energy gains are plotted in Fig 9 versus the net cavity input power (problems with the klystron modulator at the time prevented > 2 MW operation). These measurements were done at a fixed rf frequency and the bunch charge was about 20 pC so the beam loading was very small. For low average heating, the cavity detuning was about -20 kHz and for high average heating, it was about -4 kHz at the beginning of the pulse and around - 6 kHz by the end of the pulse. The gradient versus power fits agree to within the roughly 4% systematic errors so no significant gradient changes were observed as expected from Fig 8. These measurements will be repeated for power levels up to 4 MW (15 MV/m gradients).

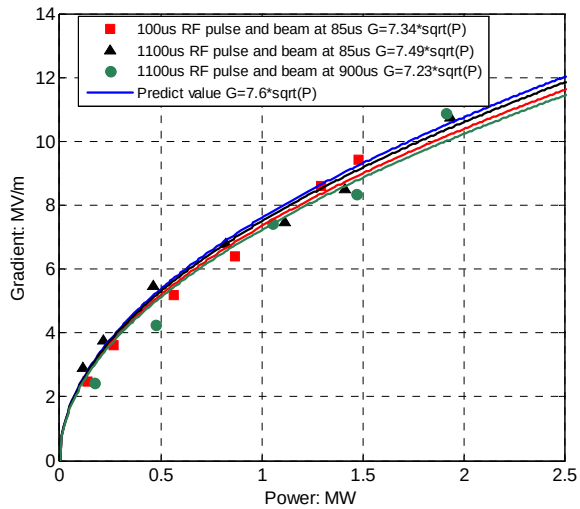

Figure 9: Single bunch acceleration gradient versus the net cavity input power (forward – reflected) for different pulse widths and bunch injection times.

SUMMARY AND OUTLOOK

A 5-cell SW cavity has been conditioned to 15 MV/m with 1ms pulses although the ultimate breakdown rate has yet to be fully characterized. As expected, detuning from average and inter-pulse heating had a small effect on the gradients achieved during single bunch operation.

In the ILC, the positron capture cavity will need to operate in a 0.5 T solenoidal magnet. Such a magnet has been installed around the 5-cell prototype to gauge its effect on the cavity performance. Although the outgassing and breakdown rate initially increased, the performance improved with rf processing. In the next few months, rf conditioning in the presence of the magnetic field will continue, breakdown location studies will be done, and the breakdown dependence on pulse width will be measured.

REFERENCES

[1] J.W. Wang, C. Adolphsen, et al., 'Studies of Room Temperature Accelerator Structures for the ILC Positron Source', SLAC-PUB-11767.

[2] J.W. Wang, C. Adolphsen, et al., 'Positron Injector Accelerator and RF System for the ILC', SLAC-PUB-12412.

[3] G. Bowden, 'L-Band Accelerator Cooling', SLAC ILC ME Note 2-05, Aug. 2005.

[4] F. Wang, 'Breakdown Characteristics Study of an 18 Cell X-band Structure', AAC08.